International Journal of Biological, Life and Agricultural Sciences
ISSN: 2415-6612
Vol:11, No:7, 2017

Inulinase Immobilization on Functionalized Magnetic Nanoparticles Prepared with Soy Protein Isolate Conjugated Bovine Serum Albumin for High Fructose Syrup Production

Homa Torabizadeh, Mohaddeseh Mikani

Abstract**—**Inulinase from *Aspergillus niger* was covalently immobilized on magnetic nanoparticles (MNPs/Fe_3O_4) covered with soy protein isolate (SPI/Fe_3O_4) functionalized by bovine serum albumin (BSA) nanoparticles. MNPs are promising enzyme carriers because they separate easily under external magnetic fields and have enhanced immobilized enzyme reusability. As MNPs aggregate simply, surface coating strategy was employed. SPI functionalized by BSA was a suitable candidate for nanomagnetite coating due to its superior biocompatibility and hydrophilicity. Fe_3O_4@SPI-BSA nanoparticles were synthesized as a novel carrier with narrow particle size distribution. Step by step fabrication monitoring of Fe_3O_4@SPI-BSA nanoparticles was performed using field emission scanning electron microscopy and dynamic light scattering. The results illustrated that nanomagnetite with the spherical morphology was well monodispersed with the diameter of about 35 nm. The average size of the SPI-BSA nanoparticles was 80 to 90 nm, and their zeta potential was around −34 mV. Finally, the mean diameter of fabricated Fe_3O_4@SPI-BSA NPs was less than 120 nm. Inulinase enzyme from *Aspergillus niger* was covalently immobilized through gluteraldehyde on Fe_3O_4@SPI-BSA nanoparticles successfully. Fourier transform infrared spectra and field emission scanning electron microscopy images provided sufficient proof for the enzyme immobilization on the nanoparticles with 80% enzyme loading.

Keywords**—**High fructose syrup, inulinase immobilization, functionalized magnetic nanoparticles, soy protein isolate.

I. Introduction

IN recent years, nanobiotechnology has gained increasing interest because of its wide range of applications including enzyme immobilization. Nanoparticles commonly vary in size from 10 to 1000 nm [1], [2]. Enzyme immobilization by using nanostructures enhances functional surface area for enzyme loading, reduces diffusion limitations and raises catalytic efficiency due to improvement of particle mobility [3], [4]. Native enzymes generally have insufficient stability against high temperature and pH variations [5], [6]. As a result, there is a great demand for ways to enhance the stability and reusability of the enzyme. Enzyme immobilization offers many advantages for industrial applications because of convenience in control, and ease of enzyme separation from the reaction mixture and recycling, to reduce product cost and enhance thermal and pH enzyme stability [7], [8]. An essential requirement for immobilization of enzyme is that the carrier should supply a biocompatible and inert environment, i.e. it should not interfere with the enzyme native structure, and thus its biological activity is well retained [9].

Among possible candidates for carrier-bound immobilization of the enzymes, MNPs are promising owing to their unique physical and chemical properties such as low toxicity, biocompatibility, superparamagnetism, large surface-to-volume ratio, easy separation under external magnetic fields, and above all their magnetic properties. MNPs with various surface modifications have been applied as the carrier for enzyme immobilization [10]-[13]. Recently, the construction of versatile core–shell MNPs has been established by physical or chemical modification of natural biopolymers on the surface of Fe_3O_4 nanoparticles for functionalizing of these particles. Amongst the commonly used biopolymers, proteins are considered to be one of the most substantial materials for functionalizing MNPs owing to their active surface which is mostly attributed to ε-NH_2 group of lysine amino acid residues as well as superior biocompatibility and their hydrophilic properties. Magnetic iron oxide nanoparticles have hydrophobic surfaces with a large surface area/volume ratio. Thus, in the absence of any surface coating, these particles tend to form aggregates due to hydrophobic interactions and result in an increase in particle size. Moreover, protein nanoparticle utilization for nanomagnetite coating enhances the functional surface area of coated Fe_3O_4, and therefore, it increases enzyme loading [14]-[16]. In this research, it was attempted to inulinase immobilization via covalent binding with SPI-BSA nanoparticles coated on iron oxide nanoparticles. The preparation of Fe_3O_4@SPI-BSA@inulinase nanoparticles has been discussed in detail.

II. Materials and Methods

A. Materials and Apparatus

Inulinase from *Aspergillus niger* was obtained from Sigma-Aldrich, glutaraldehyde (%25 v/v in water), sodium potassium tartrate, SPI, and BSA were purchased from Merck. All other reagents and solvents used were of analytical grade and obtained from Merck and Sigma–Aldrich.

H. Torabizadeh is with the Iranian Research Organization for Science and Technology, Tehran, Iran (corresponding author, phone: +9821-5627-6637; fax: +9821-5627-6265; e-mail: htoraby@ alumni.ut.ac.ir).

M. Mikani was MSc student of Iranian Research Organization for Science and Technology, Tehran, Iran (e-mail: mmikani63@gmail.com).

Dynamic light scattering (DLS) method was extensively employed for sizing protein NPs in liquid phase using a BI-200 SM Goniometer Version 2 (Brookhaven Instrument Corp., Holtsville, NY, USA). The light scattered by the NPs was detected at 173°, in dynamic laser scattering. For electrophoretic mobility determination, which is the relation between the NPs velocity and the electric applied field, size distribution and mean size were calculated. In addition, zeta potential was measured by DLS method and was used to investigate nanoparticles stability against aggregation. Surface analysis was done using a low vacuum Tescan Mira II Field emission scanning electron microscope (FE-SEM, Czech Republic) after coating the samples with a thin layer of gold by magnetron sputtering. Energy-dispersive X-ray spectrometry (EDX, EDS) is an important non-destructive analytical tool mostly applied for the chemical composition. For evaluation of absorbance intensity spectrophotometer (Perkin Elmer Lambda 25 UV/VIS, United States) was applied. Infrared spectra of all formulations were recorded with Fourier transform infrared spectroscopy (FTIR-8300, Shimadzu, Japan). The nanoparticles were lyophilized before FT-IR analysis. The spectra were averaged and smoothed, and their baselines were calibrated with the Spectra Manager software. The nature of Fe_3O_4@SPI-BSA NPs was studied using the FTIR characterization method between 400 and 4000 cm^{-1} before and after enzyme immobilization. FTIR spectra of KBr pellets formed from dry powder samples of Fe_3O_4@SPI-BSA NPs precursor were taken.

All the values expressed were mean standard deviation of three replicate experiments.

B. Magnetite Nanoparticles (MNPs) Preparation

MNPs were synthesized by co-precipitation method. A ferric and ferrous ions mixture solution in a 1:2 molar ratio was made ready. At first, 8.86 gr $FeCl_3$-$6H_2O$ (99% purity) and 3.25 gr $FeCl_2$-$4H_2O$ (99% purity) were dissolved in 400 mL of deionized water in a three-necked flask. The flask was under nitrogen atmosphere and then, 10 ml sodium hydroxide solution was dropped into flask under constant stirring. After mixing the solution, the color of it changed from light brown to black, indicating the forming of Fe_3O_4 nanoparticles. The resultant Fe_3O_4 nanoparticles were separated by external magnetic field, and then washed with water for three times. Finally, the magnetic Fe_3O_4 nanoparticles were dispersed in deionized water [17]-[20]. The reaction principle is as follows:

$$2Fe^{3+} + Fe^{2+} + 8OH^- \rightarrow Fe_3O_4 + 4H_2O \quad (1)$$

The morphology and the size of nanomagnetite were analyzed by using field emission scanning electron microscopy.

C. SPI Nanoparticles Fabrication

Desolvation technique was employed for preparation of SPI nanoparticles. At first, SPI powder at concentrations of 1.5 to 4 mg/mL was dissolved in deionized water and its pH was adjusted to 9.0 with 0.1 and 1.0 M NaOH solution during stirring. The influence of SPI concentration on the size of prepared NPs was studied using DLS method. Nanoparticles were obtained by dropwise non-solvent addition to SPI aqueous solution under constant stirring until the solution became turbid. Ethanol or acetone was applied as desolvating agents, and the size of attained NPs were compared. In this project, desolvation method was accomplished by sonication technique (400 Hz, 10 min, 25±5 ^{0}C). Finally, the resulting SPI nanoparticles were crosslinked with 380 µl of glutaraldehyde (25% V/V in water). Then, 470 µl of Tween-80 was added to block the non-reacted aldehyde functional group and stabilize the preparation. Large aggregates were eliminated by centrifuge at 13,000 rpm for 15 min [21]-[26]. The particle size and size distribution of SPI NPs were determined by FE-SEM, and DLS techniques. Zeta potential of the SPI NPs was determined by DLS.

D. Synthesis of Fe_3O_4/SPI/BSA Nanostructure

After optimizing of the SPI concentration in SPI NPs fabrication, BSA at different values was added to SPI NPs simultaneously and non-simultaneously for preparing hybrid protein NPs. In simultaneous addition, the BSA powder was added at different concentrations to SPI powder, and then desolvating agent was applied to prepare hybrid SPI-BSA NPs. The method was the same as preparation of SPI NPs. In contrast, in non-simultaneous addition, SPI and BSA NPs was made separately, and then mixed to each other.

E. Fe_3O_4@SPI-BSA NPs Carrier Preparation

First, 0.06 gr of SPI-BSA NPs and 400 µl gluteraldehyde were dissolved in 50 ml of 0.1 M phosphate buffer solution pH 7.0 and then, 0.1 gr of MNPs was added. After that, ultrasound technique with 300 Hz frequency was applied for hybrid SPI-BSA NPs binding directly onto MNPs for 10 minutes at room temperature then, kept at ambient temperature overnight. Thereafter, the Fe3O4@SPI-BSA NPs obtained were isolated centrifugally at 13,000 rpm and washed with deionized water to eliminate the unreacted SPI-BSA NPs as much as possible [15], [16].

F. Immobilization of inulinase Enzyme on the Fe_3O_4@SPI-BSA NPs

The covalent inulinase enzyme immobilization was done by mixing enzyme solution and Fe_3O_4@SPI-BSA NPs, and stirring for 24 hrs at 4 °C. Gluteraldehyde as a cross linker (25 mg/mL aqueous solution), for covalent attachment, was applied, in 50 mM sodium acetate buffer at pH, 5.4 [7], [8], [27].

III. Results and Discussion

A. Fe_3O_4@SPI-BSA@inulinase Preparation and Morphological Characterization Study

At first step, the morphology and size of the fabricated MNPs were investigated using FE-SEM. The FE-SEM image of the prepared MNPs and size distribution graph were shown in Figs. 1 (A) and (B).

The obtained water-based MNPs possessed spherical

morphology, they are uniformly distributed, and the mean diameter of nanomagnetite is less than 50 nm. The existence of the MNPs was confirmed by means of EDX which determined the elemental composition of Fe_3O_4 (Fig. 2).

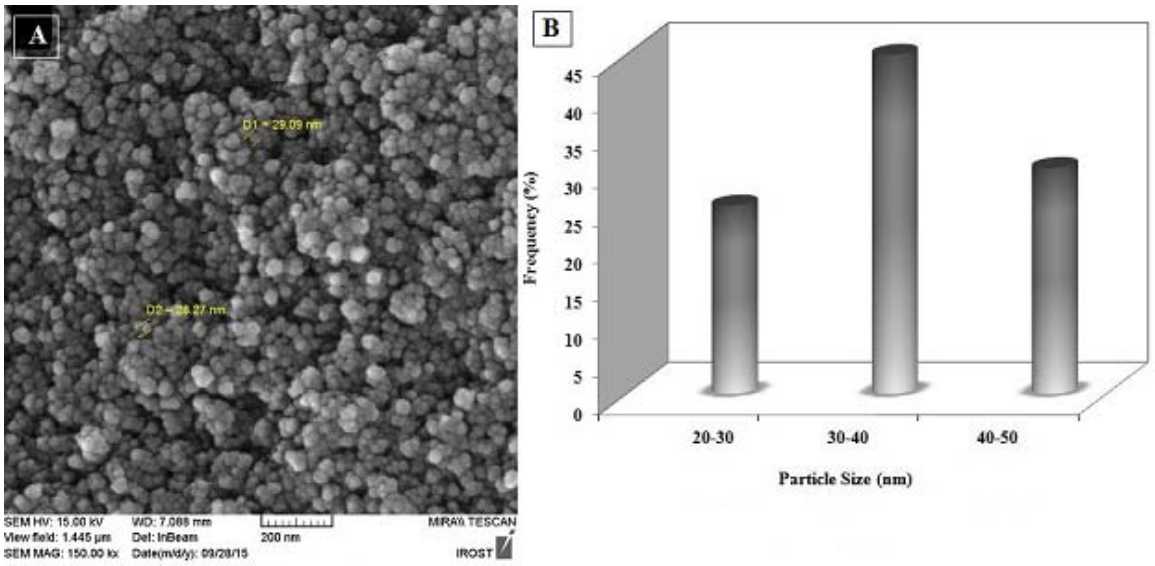

Fig. 1 (A) FE-SEM image of the nanomagnetite, (B) the nanomagnetite size distribution

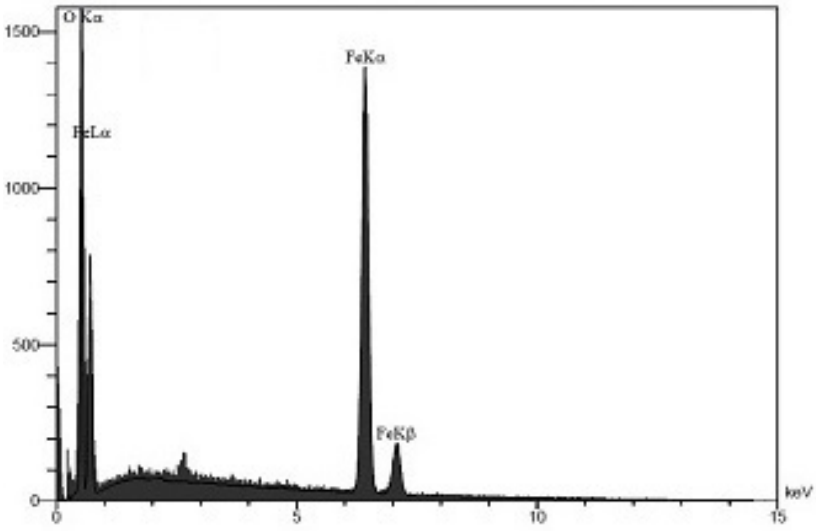

Quantitative Results

El	Line	Int	Error	K	Kr	W%	A%	ZAF	Formula	Ox%	Cat#
O	Ka	351.4	145.3040	0.2127	0.1862	26.02	55.12	0.7156		0.00	0.00
Fe	Ka	748.2	1.1838	0.7873	0.6894	73.98	44.88	0.9319		0.00	0.00
				1.0000	0.8756	100.00	100.00			0.00	0.00

Fig. 2 The EDX for elemental composition of Fe_3O_4

B. SPI NPs Fabrication at the Optimized Condition

Comparative study of the effect of SPI concentration on NPs size and distribution for two types of desolvating agents (ethanol and acetone) was performed (Fig. 3 (A)). The influence of initial SPI concentration on NPs size is demonstrated in Fig. 3 (B). The results are obtained from DLS results of size distributions and log normal size distributions of SPI NPs that are formed at the optimized initial SPI concentration in acetone environment as desolvating agent (Figs. 3 (C) and (D)).

As it is implied in Fig. 3, by increasing the initial SPI concentration from 1.5 to 4 mg/ml resulted in an increase in particle size. This difference might be attributed to the fact that higher protein concentration favored the collision and aggregation of protein molecules [23]. The concentration of SPI in the initial solution is a significant factor in the particle formation process, which might be explained by considering the classical theory of nucleation. The optimum SPI concentration was 2 mg/ml. The results obtained for two different desolvating agents showed that particle size increases with the use of ethanol.

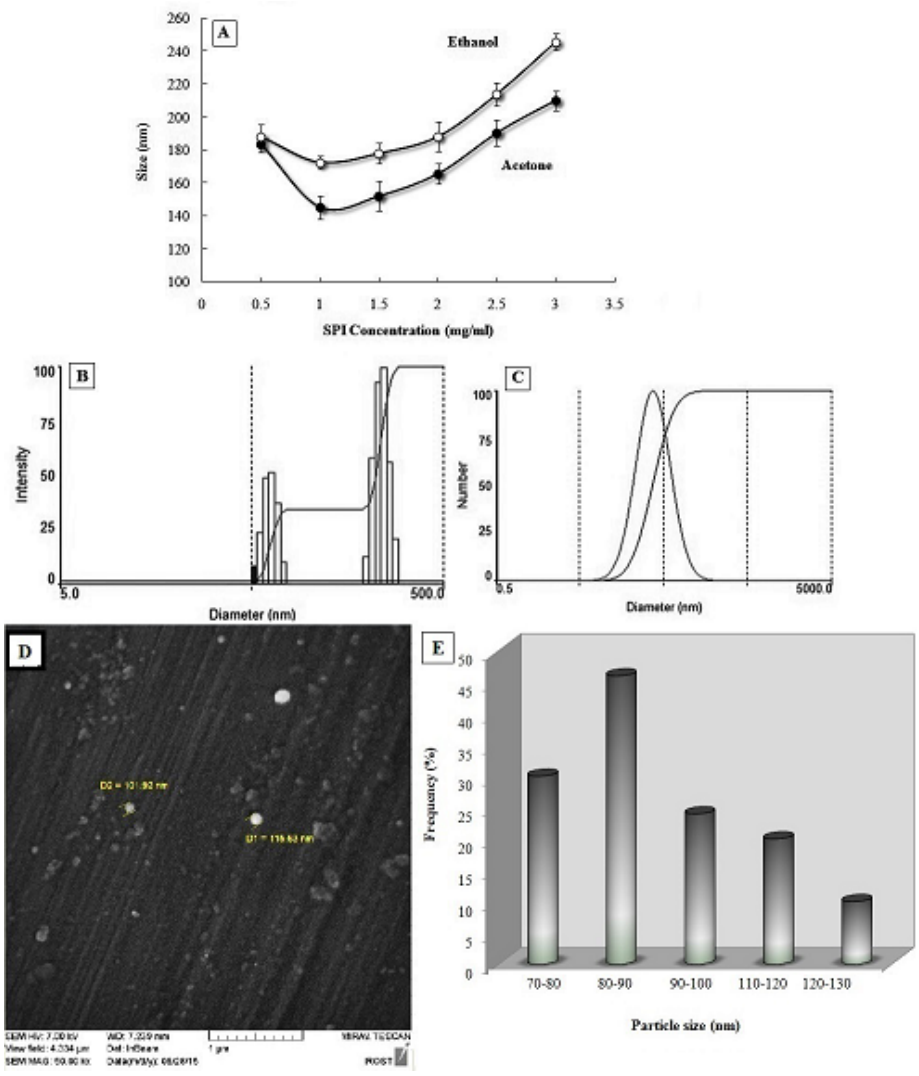

Fig. 3 (A) The effect of SPI concentration on the size of soy protein nanoparticles at two types of desolvating agents based on DLS results, (B and C) log normal size distributions of SPI NPs formed at the optimized initial SPI concentration and aceton as desolvating agent, (D) FE-SEM image of the SPI nanoparticles, (E) the SPI nanoparticles size distribution based on DLS results

The size range of SPI NPs prepared by using acetone was lower for all SPI concentrations tested (1.5-4 mg/mL). The particle distribution profiles from DLS confirm that acetone is a better desolvating agent to produce uniform NPs from SPI. The nanoparticulation efficiency results show that acetone is a more efficient solvent to convert SPI molecules into NPs. Organic solvents such as acetone and ethanol have the ability to promote nucleation and precipitation of the SPI molecules to aggregate because SPI is insoluble in them and the aggregation process results spontaneously in NPs [22], [23], [25], [26].

The morphology of SPI nanoparticles that were characterized by FE-SEM method is illustrated in Fig. 3 (D). The size of nanoparticles ranged from 80 to 130 nm (Fig. 3 (E)). The FE-SEM images of lyophilized NPs confirmed the DLS results, but the effective diameter of the particles using DLS measurement was a little bigger than results from FE-SEM image. This difference was possibly due to the shrinkage caused by the cast-drying process as well as the vacuum environment in FE-SEM image [23]. It was obvious that most

of the resulting SPI NPs morphologies were semispherical.

C. Hybrid SPI-BSA NPs Fabrication

In the next step, the effect of SPI to BSA ratio versus size of produced SPI-BSA NPs was analyzed. The addition of BSA to SPI was performed by two different conditions, simultaneously and non-simultaneously. In simultaneous method, the prepared SPI and BSA solutions that were subjected to the ultrasonic waves crashing were added together to the desolvation environment, while in non-simultaneous procedure, at first SPI solution is prepared, and then, BSA solution will be added to SPI containing earlier environment. The results were shown in Fig. 4. In the simultaneous procedure, the SPI-BSA NPs size decreased from %12.5 to %37.5 BSA and increased %37.5 to %100 BSA concentration, while in the non-simultaneous procedure the SPI-BSA NPs size decreased from %12.5 to %50 BSA and increased 50 to %100 BSA concentration, respectively. In the simultaneous process, the size range of SPI-BSA NPs was lower for all %BSA compared with the non-simultaneous process.

DLS results of size distributions and log normal size distributions of SPI-BSA NPs formed at the optimized simultaneous and non- simultaneous procedures were shown in Figs. 5 (A)-(D).

In the effect of BSA concentration in hybrid SPI-BSA NPs on zeta potential (Fig. 4), as indicated, by adding BSA to SPI, zeta potential also increases with increasing BSA concentration. These changes can be attributed to the negative surface charge of BSA molecules resulting in a gradual increase in electrostatic repulsion between the nanoparticles and a decrease in aggregation of particles. NPs with a zeta potential above +/-30 mV have been shown to be stable in suspension, as the surface charge prevents aggregation of the particles [27], [28]. Eventually, according to the obtained results in determining the hybrid SPI-BSA NPs size and zeta potential, the optimum amount for adding BSA to SPI in a simultaneous process was selected 37.5%.

D.FE-SEM Study of Hybrid SPI-BSA NPs

The morphology and the hybrid SPI-BSA NPs size were investigated by the FE-SEM measurement. The SPI-BSA NPs possessed spherical morphology (Fig. 7 (A)). FE-SEM images showed that SPI-BSA NPs were found to be in the range of 70-100 nm and mean size of about 85 nm. The particle size distribution of SPI-BSA NPs is shown in Fig. 7 (B).

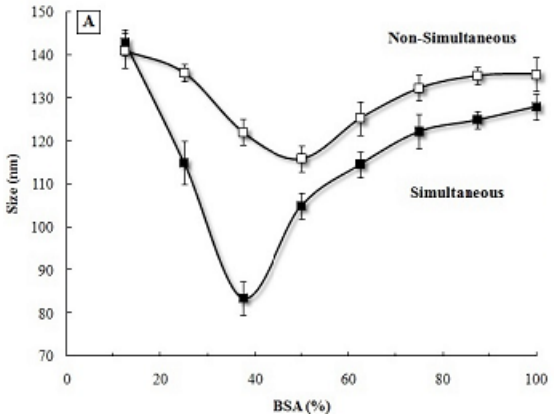

Fig. 4 Effect of BSA concentration at simultaneous and non-simultaneous process on the size of SPI-BSA nanoparticles based on DLS results

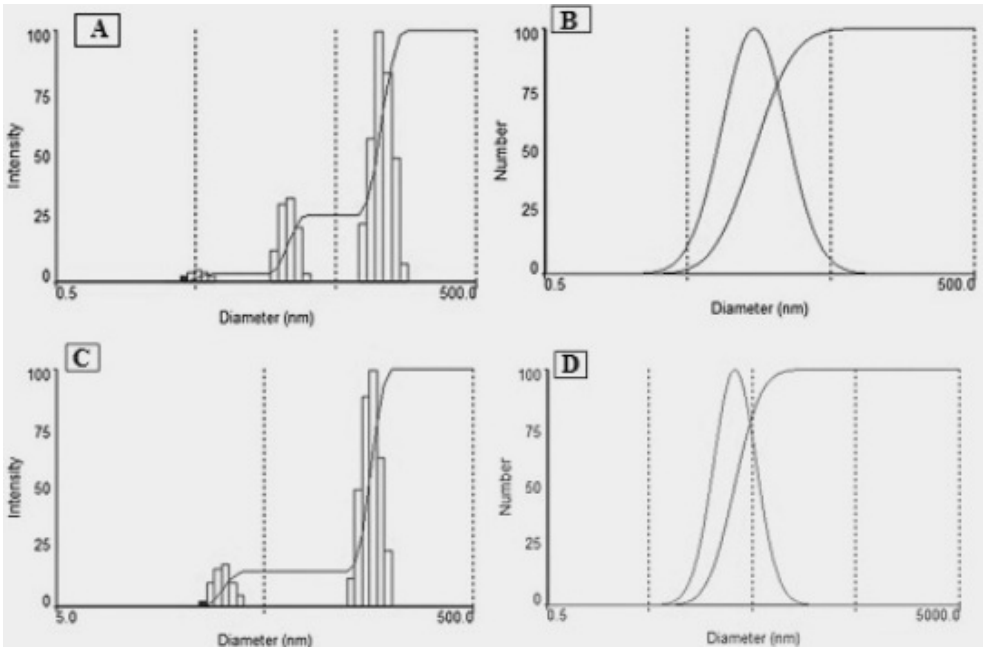

Fig. 5 (A), (B) DLS results of size distributions, (C), (D) and log normal, size distributions of SPI-BSA NPs formed at the optimized simultaneous and non- simultaneous procedures

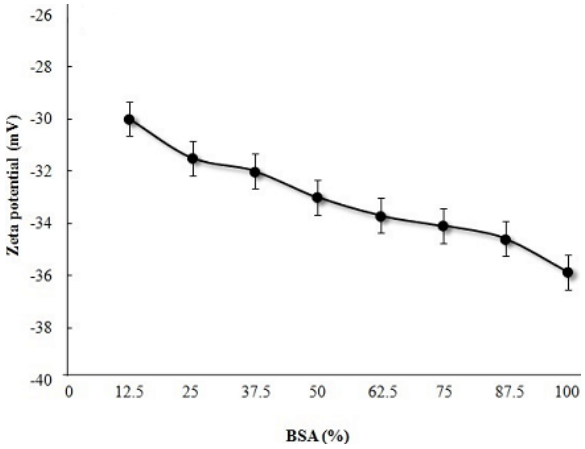

Fig. 6 The effect of BSA concentration on zeta potential of SPI-BSA nanoparticles

E. UV-Vis Spectra of Fabricated Hybrid SPI-BSA NPs

SPI NPs protein possessed two main absorbance peaks in the UV-Vis region, one between 215-230 nm, where peptide bonds absorb, and another at about 280 nm due to light absorption by aromatic amino acids (i.e., tyrosine, tryptophan and phenylalanine) (Fig. 5 (B)) [29], [30].

The results revealed that, after addition of 0.25-1 mg.ml^{-1} BSA to 1 mg.ml^{-1} SPI during nanoparticle preparation, peptide bonds and aromatic amino acids are reinforced. Moreover, it is specified that the protein structure of the nanoparticles is preserved during nanoparticle preparation.

F. Fe_3O_4@SPI-BSA@inulinase Characteristics

As shown in Fig. 6 (A), the revealed feature of Fe_3O_4@SPI-BSA NPs confirmed that high surface and uniform distribution were extended through the surface which was believed to play a significant role in enzyme immobilization. The mean diameter of Fe_3O_4@SPI-BSA NPs was less than 120 nm, which was higher than the naked nanomagnetite. The size difference demonstrated that the SPI-BSA NPs was coated on MNPs successfully. After coating a shell of SPI-BSA, the resultant Fe_3O_4@SPI-BSA NPs were still spherical with the size increased to about 90-120 nm.

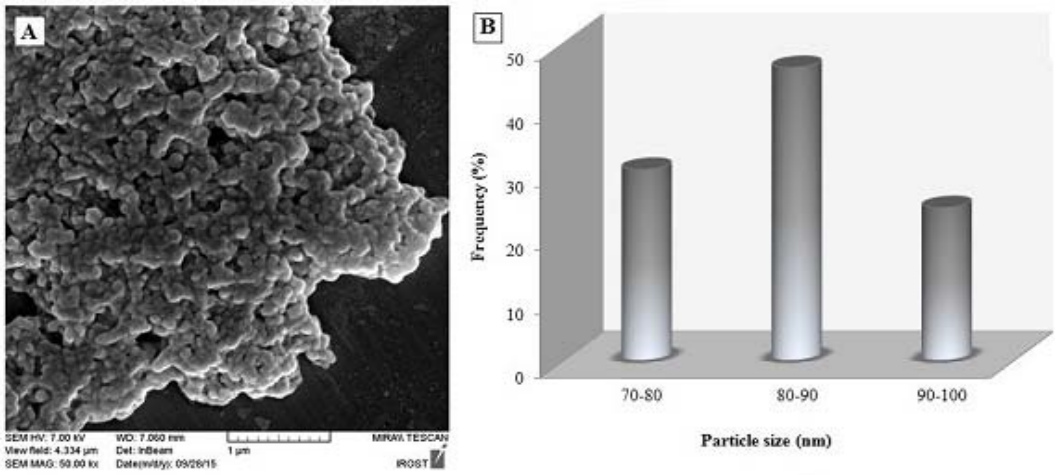

Fig. 7 (A) FE-SEM image of the SPI-BSA NPs, (B) the SPI-BSA NPs size distribution

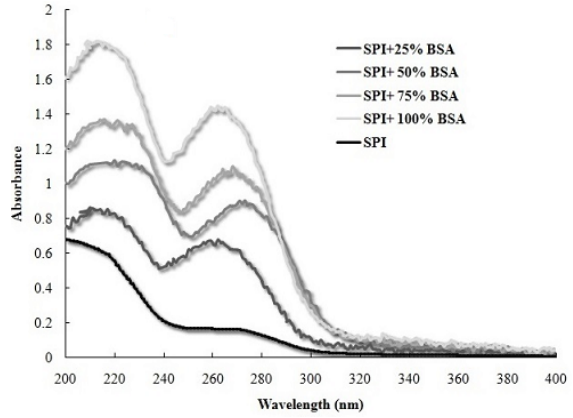

Fig. 8 The UV-Vis spectra of SPI-BSA NPs at different BSA concentrations

The particle size distribution graph is shown in Fig. 6 (B). Finally, the FE-SEM image indicated the successful immobilization of inulinase on Fe_3O_4@SPI-BSA NPs which retained its activity and natural structure that is required to improve inulin hydrolysis in industrial media.

G. Fourier Transform Infrared Spectroscopy (FTIR)

As can be seen in Fig. 10, the spectrum before enzyme immobilization indicated Fe-O stretching vibration at 600 cm^{-1}, the adsorbed water molecules stretching at 1621 cm^{-1} and an intense OH band around 3400 cm^{-1}.

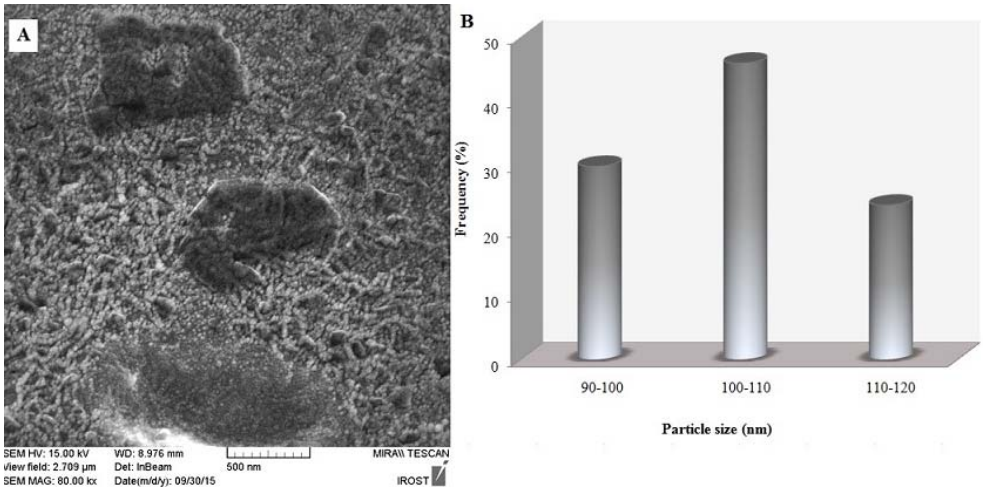

Fig. 9 (A) FE-SEM image of the immobilized enzyme on the NPs, (B) the Fe_3O_4@SPI-BSA NPs size distribution

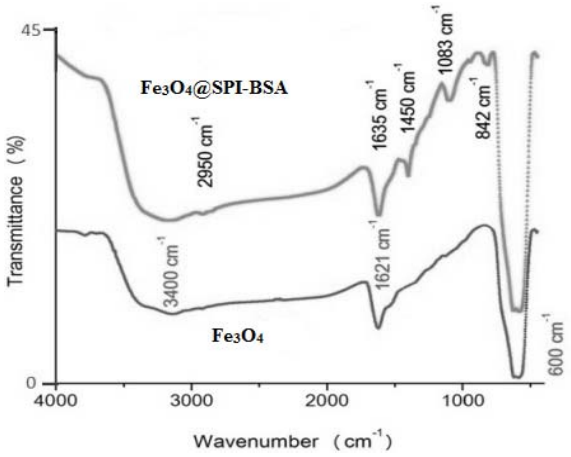

Fig. 10 FTIR spectrum of Fe_3O_4 nanostructure before and after coating by SPI-BSA NPs

The OH band was corresponding to the stretching vibrations of Fe-OH groups attached on the Fe_3O_4 surface and also can be pointed to the remaining water that was not omitted from the nanomagnetite surface. The SPI peaks at 1450 cm^{-1}, 2950 cm^{-1}, and 1635 cm^{-1} were attributed to the stretching vibration mode of C=O, N-H, COO^- bonds, respectively. The significant peak of BSA at 1637 cm^{-1} was corresponding to the vibrations of the backbone C=O belonging to the vibration of amide groups in FTIR spectrum overlapped by Fe_3O_4 peak. After enzyme immobilization, the peaks at 1253, 1522, 2950 cm^{-1} attributed to the stretching vibration of C-O-C, bending vibration of N-H and stretching vibration of C-H, respectively [23], [29], [34], [35].

H.Enzyme Loading

Enzyme immobilization appears as a key factor to improve reutilization, thermal stability and reusability. Immobilized enzymes should preserve their structure, function, and their biological activity after immobilization, stay tightly bound to the surface of the carrier and not leached during the use of enzyme. It usually eliminates most of the disadvantages for application of free enzymes in industrial processes [14], [15]. Nanoparticles provide large surface area per unit mass for high enzyme loading. The enzyme loading capacity (ELC) is estimated via using (2).

$$Q=\frac{(C_1-C_2)V}{W} \quad (2)$$

where Q is the value of enzyme loading (mg enzyme per mg support). C_1 is protein concentration in the inulinase solution before immobilization. C_2 is the protein concentration of the residual free enzyme in the cocktail after immobilization. V is the total solution volume and W is the weight of carrier (mg). The protein content of inulinase was determined by using Bradford's method [31]-[33]. The results of this study indicated that the enzyme loading under described immobilization conditions was nearly 80%.

IV. Conclusion

On the whole, MNPs were synthetized by co-precipitation method, and subsequently their surface was coated with SPI-BSA NPs to procreate particles with high sustainability. Small and more uniform spherical SPI-BSA nanoparticles with 70-100 nm diameter were produced by using of acetone as desolvating agent. The initial SPI concentration as a precursor for SPI NPs preparation was optimized, then for increasing surface lysine residues and promoting zeta potential, BSA NPs were utilized at various concentrations by simultaneous and non-simultaneous procedures. In simultaneous process, the size range of SPI-BSA NPs was lower for all BSA concentrations compared with non-simultaneous process, and in simultaneous procedure at 37.5% BSA composed nanopaticle size was obtained 83.5 nm. The zeta potential of the NPs dispersion was −34 mV, which revealed good stability. The synthesized SPI-BSA NPs displayed a spherical structure. The Fe_3O_4@SPI-BSA NPs were then evaluated for enzyme immobilization capability, and the highest loading efficiency of about 80% was achieved.

ACKNOWLEDGEMENT

The financial support provided by Iranian Research Organization for Science and Technology (IROST) and Iran Nanotechnology Initiative Council (INIC) is greatly acknowledged.

REFERENCES

[1] R. Couvreur, R. Gref, K. Andrieux, K, and C. Malvy, C, "Nanotechnologies for drug delivery: Application to cancer and autoimmune diseases," *Prog. Solid State Chem*., vol. 34, pp. 231-235, Jul. 2006.

[2] S. Kumaresh, T. M Aminabhavi, A. R Kulkarni, and W. E Rudzinski, "Biodegradable polymeric nanoparticles as drug delivery devices," *J. Control. Release*., vol. 70, pp. 1-20, Jan. 2001.

[3] T. Xie, A. M Wang, L. F Huang, H. F Li, Z. M Chen, and Q. Y Wang, "Recent advance in the support and technology used in enzyme immobilization," *Afr. J. Biotechnol*., vol. 8, pp. 4724–4733, Oct. 2009.

[4] H. Jia, G. Zhu, and P. Wang, "Catalytic behaviors of enzymes attached to nanoparticles: the effect of particle mobility," *Biotechnol. Bioeng*., vol. 84, pp. 406-414, Nov. 2003.

[5] S. Datta, L. R. Christena, Y. Rani, and S. Rajaram, "Enzyme immobilization: An review on techniques and support materials," *Biotechnol*., vol. 3, pp. 1-9, Feb. 2012.

[6] R. A. Sheldon, "Enzyme immobilization: The quest for optimum performance," *Adv. Synth. Catal*., vol. 349, pp. 1289-1307, Jun. 2007.

[7] H. Torabizadeh, M. Tavakoli, and M. Safari, "Immobilization of thermostable α-amylase from Bacillus licheniformis by cross-linked enzyme aggregates method using calcium and sodium ions as additives," *J. Mol. Catal. B: Enzym*., vol.108, pp. 13-20, Jun. 2014.

[8] A. Richetti, C. B. Munaretto, L. A. Lerin, L. Batistella, J. V. Oliveira, R. M. Dallago, V. Astolfi, M. D. Luccio, M.A. Mazutti, D. D. Oliveira, and H. Treichel, "Immobilization of inulinase from *Kluyveromyces marxianus* NRRL Y-7571 using modified sodium alginate beads," *Bioprocess and Biosys. Eng*., vol. 35, pp. 383-388, Aug. 2012.

[9] D. T. Mitchell, S. B. Lee, L. Trofin, N. Li, T. K. Nevanen, H. Soderlund, C. R. and martin, "Smart nanotubes for bioseparations and biocatalysis," *J. Am. Chem. Soc*., vol. 124, pp. 11864–11865, Oct. 2002.

[10] L. H. Reddy, J. Arias, J. Nicolas, and P. Couvreur, "Magnetic nanoparticles: Design and Characterization, Toxicity and Biocompatibility. Pharmaceutical and Biomedical Applications," *Chem. Rev*., vol. 112, pp. 5818-5878, Oct. 2012.

[11] G. Couto, J. Klein, W. Schreiner, D. Mosca, A. Oliveira, and A. Zarbin, "Nickel nanoparticles obtained by a modified polyol process: Synthesis, Characterization, and Magnetic Properties," *J. Colloid Interface Sci*., vol. 311, pp. 461-468, Jul. 2007.

[12] C. Sun, J. Lee, and M. Zhang, "Magnetic nanoparticles in MR imaging and drug delivery. *Adv. Drug Deliv. Rev*., vol. 60, pp. 1252-1265, Apr. 2008.

[13] X. Liang, H. Shi, X. Jia, Y. Yang, and X. Liu, "Dispersibility, shape and magnetic properties of nano-Fe_3O_4 particles," *Mater. Sci. Appl*., vol. 2, pp. 1644-1653, Mar. 2011.

[14] A. Gupta, and M. Gupta, "Synthesis and surface engineering of iron oxide nanoparticles for biomedical applications," *Biomaterials*., vol. 26, pp. 3995-4021, Jun. 2005.

[15] M. Mikhaylova, D. K. Kim, C. Catherine, and S. G. Adam, "BSA immobilization on amine-functionalized superparamagnetic iron oxide nanoparticles," *Chem. Mater*., vol. 16, pp. 2344-2354, Sep. 2004.

[16] L. Zhanfeng, Q. Linhui, Z. Shuangling, W. Hongyan, and C. Xuejun, "Synthesis and characterization of monodisperse magnetic Fe_3O_4@BSA core–shell nanoparticles," *Colloids Surf*., vol. 436, pp. 1145-1151, Sep. 2013.

[17] I. Nedkov, T. Merodiiska, L. Slavov, R. E. Vandenberhe, Y. Kusano, and J. Takada J, "Surface oxidation, size and shape of nano-sized magnetite obtained by co-precipitation," *J. Magn. Magn. Mater*., vol. 300, pp. 358-367, Nov. 2006.

[18] H. Itoh, and T. Sugimoto, "Systematic Control of Size, Shape, Structure, and Magnetic Properties of Uniform Magnetite and Maghemite Particles," *J. Colloid. Interface. Sci*., vol. 12, pp. 283–295, Sep. 2003.

[19] M. C. Mascolo, Y. Pei, and T. A. Ring, "Room temperature co-precipitation synthesis of magnetite nanoparticles in a large pH window with different bases," *Materials*., vol. 6, pp. 5549-5567, Nov. 2013.

[20] N. D. Kandpal, S. Sah, R. Loshali, R. Joshi, and J. Prasad, "Copercipitation method of characterization of iron oxide nanoparticles," *J. Sci. Ind. Res*., vol. 73, pp. 87-90, Feb. 2014.

[21] W. Lohcharoenkal, L. Wang, Y. C. Chen, and Y. Rojanasakul, "Protein nanoparticles as drug delivery carriers for cancer therapy," *J. Biomed. Biotechnol*., vol. 2014, pp. 1-15, Jan. 2014.

[22] C. Weber, C. Coester, J. Kreuter and K. Langer, "Desolvation process and surface characterization of protein nanoparticles," *Int. J. Pharm*., vol. 194, pp. 91-102, Jan. 2000.

[23] Z. Teng, Y. Luo, and Q. Wang, "Nanoparticles synthesized from soy protein: Preparation, characterization, and application for nutraceutical encapsulation," *J. Agric. Food. Chem*., vol. 60, pp. 2712-2720, Mar. 2012.

[24] S. A Krishna, P. Amareshwar, and P. Chakravarty, "Different techniques used for the preparation of nanoparticles using natural polymers and their application," *J. Pharm. Pharm. Sci*., vol. 3, pp. 45-50, Oct. 2011.

[25] J. Y. Jun, H. H. Nguyen, S. Y. R. Paik, H. S. Chun, B. C. Kang, and S. Ko, "Preparation of size-controlled bovine serum albumin (BSA) nanoparticles by a modified desolvation method," *Food. Chem*., vol. 4, pp. 1892-1898, Dec. 2011.

[26] F. Galisteo-González and J. A. Molina-Bolívar, "Systematic study on the preparation of BSA nanoparticles," *Colloids Surf., B*., vol. 123, pp. 286-292 Nov. 2014.

[27] R. Mehravar, M. Jahanshahi, and N. Saghtoleslami, "Fabrication and evaluation of human serum albumin (HAS) nanoparticles for drug delivery application," *Int. J. Nanosci*., vol. 8, pp. 319–322, Nov. 2009.

[28] M. Jahanshahi, G. D. Najafpour, and M. Rahimnejad, "Applying the Taguchi method for optimized fabrication of bovine serum albumin (BSA) nanoparticles as drug delivery vehicles," *Afr. J. Biotechnol*., vol. 7, pp. 362-367, Feb. 2008.

[29] D. A. Skoog, F. J. Holler, and S. R. Crontch, Principles of instrumental analysis, Thomson Brooks/Cole, Canada, 2007, pp. 237-250.

[30] P. Singh, P. K. and Gill, "Production of inulinases: Recent advances," *Biotechnol.,* vol. 44, pp. 151-162, Feb. 2006.

[31] T. M. Mohamed, S. M. El-Souod, E. M. Ali, M. O. El-Badry, and M.M. El-Keiy, "Immobilization and characterization of inulinase from Ul ocladium atrumon nonwoven fabrics," *J. Biosci*., vol. 39, pp. 785–793, Nov. 2014.

[32] M. M. Bradford, "A rapid and sensitive method for the quantitation of microgram quantities of protein utilizing the principle of protein-dye binding," *Anal. Biochem*., vol. 72, pp. 248–254, May. 1976.

[33] H. Torabizadeh, M. Habibi-Rezaei, M. Safari, A. A. Moosavi-Movahedi, and H. Razavia, "Semi-rational chemical modification of endoinulinase by pyridoxal 5′-phosphate and ascorbic acid," *J. Mol. Catal. B: Enzym*, vol. 62, pp. 257-264, Mar. 2010.

[34] S. Sundar, J. Kundu and S. C. Kundu, "Biopolymeric nanoparticles," *Sci. Tech. Adv. Mater*., vol. 11, pp. 1-13, Jan. 2010.

[35] J. Zhang, L. Liang, Z. Tian, L. Chen, and M. Subirade, "Preparation and in vitro evaluation of calcium-induced soy protein isolate nanoparticles and their formation mechanism study," *Food Chem*., vol. 133, pp. 390-399, Jul. 2012.